Estuaries and Coasts (2023) 46:323–335
https://doi.org/10.1007/s12237-022-01140-3

Comparison of Spectral Wave Dissipation by Two Living Shoreline Features in a Sheltered Tidal Bay

Alexa Leone[1] · **Navid Tahvildari**[2]

Received: 28 June 2021 / Revised: 6 October 2022 / Accepted: 24 October 2022 / Published online: 14 November 2022

Abstract

Living shorelines combine structural and natural elements to mitigate coastal erosion and flood hazards by dissipating waves while providing habitat. Despite growing interest in these features, the efficiency of living shorelines in wave attenuation has not been investigated well yet. In this study, we measure the effectiveness of a marsh + stone sill feature and an array of oyster reef balls in dissipating wave energy. The two features are located along the same shoreline in a small, sheltered bay along the Lafayette River in the City of Norfolk, Virginia. This low-energy environment represents the typical condition where living shorelines are proposed as viable shore protection measures. The site was selected due to proximity of the two features which subjected them to the same wave conditions. Pressure sensors were deployed around the features for 27 days in September and October of 2019. A spectral analysis was performed to quantify energy loss across wave frequencies. The maximum significant wave height was 9 cm which was driven by dominant wind speed of 2–4 m/s coming from southwest. The tidal range was small (0.8 m) and caused the marsh sill and reef balls to be submerged 28% and 94% of the deployment time, respectively. Wave attenuation was dependent on the ratio of the significant wave height to the freeboard above structure crest (R). The threshold of 0.625 was defined to separate the results to conditions where structural features were submerged and were emergent or barely submerged. For $R > 0.625$, the marsh + stone sill and oyster reef balls attenuated waves by 40% and 13%, respectively. Both features were equally inefficient in attenuating waves if freeboard was large such that only 7% reduction in significant wave height was observed. Accounting for wave shoaling and depth-induced breaking around the marsh + stone sill shows that the stone sill is responsible for 27% of the observed wave dissipation. This study can inform coastal engineers and managers on selection of suitable living shoreline design alternatives.

Keywords Wave dissipation · Spectral analysis · Shoreline stabilization · Marsh-stone sill · Oyster reef balls · Living shorelines

Introduction

Beaches have a natural equilibrium, meaning that they naturally adjust their profile at a seasonal time scale to provide the most efficient dissipation of the incoming ocean energy. However, due to climate change, storms are likely to happen more frequently with increased intensity (e.g., Emanuel 2013) giving beaches less time to restore on their own. Adaptation strategies are developed to prepare for these extreme storms. A common approach has been to use structural systems that provide physical barriers such as sea walls or dikes to stabilize the shoreline. However, in recent years, strategies have shifted to incorporate natural elements like vegetation, oyster reefs, or sand dunes. Thus, nature-based adaptation can constitute wetland or dune restoration or implementation of hybrid features that combine structural and natural elements. These hybrid features, also called living shorelines, have used a variety of designs. A common design includes low-crested breakwaters as the structural component which primarily attenuates wave energy and protects the shoreline from erosion and wetland vegetation or submerged aquatic vegetation which acts to stabilize sediments and provide habitat for wildlife. Oyster reefs are

Communicated by Eduardo Siegle

✉ Navid Tahvildari
ntahvild@odu.edu

[1] Department of Ocean Engineering, University of Rhode Island, Kingston, USA

[2] Department of Civil and Environmental Engineering, Old Dominion University, Norfolk, USA

another example of living shorelines which have been widely used due to their ecosystem services in stabilizing or reversing shoreline erosion (e.g., Meyer et al. 1997; Scyphers et al. 2011; Wiberg et al. 2019) and enhancing water quality and economic productivity (e.g., Coen et al. 2007). In addition to ecosystem benefits, living shorelines sequester carbon away from the atmosphere, potentially making this approach to coastal resilience beneficial for mitigating climate change (Davis et al. 2015).

Living shorelines change coastal hydrodynamics in their vicinity (Whitman and Reidenbach 2012; Wiberg et al. 2019; Safak et al. 2020; Zhu et al. 2020), and predicting their success requires a detailed understanding of the flow and sediment processes around them. Nearshore waves are the main drivers of erosion in coastal and estuarine environments (Marani et al. 2011; Möller et al. 2014; Leonardi et al. 2016). Wave spectra undergo substantial change in interactions with coastal structures and bathymetry in shallow water. As waves propagate toward the shoreline, wave height transforms due to shoaling, refraction, breaking, reflection from beach slopes and structures, and diffraction (e.g., Dean and Dalrymple 2004). Increase in wave height due to shoaling in shallow waters pushes them to breaking which results in energy loss and subsequent reduction in wave height. Coastal structures also dissipate wave energy as waves break on structure slopes or as within or above the porous structures. Therefore, quantifying spectral wave attenuation by living shorelines is critical to predict their performance and will help develop optimal designs where desired coastal protection is achieved, while ecological functions are permitted through implementation of natural elements and sufficient land–water connectivity.

Despite growing interest for living shorelines as a sustainable coastal protection strategy, there have been a few studies that have quantified wave attenuation by these features. Wiberg et al. (2019) studied wave dissipation by four restored oyster reefs in the Eastern Shore of Virginia. They related reduction in wave height across oyster reefs to water depth above reef crests and reported that wave dissipation decreases with increase in the free board over the reef crest. Specifically, as water level was about the same as the reef crests, waves lost 30–50% of their height, while in higher tides where water depth was up to 0.25 m higher than reef crest, wave height was decreased by 0–20%. Wave height was reduced less than 10% for water depths higher than this threshold. In a similar study, Zhu et al. (2020) measured wave dissipation by constructed oyster reefs in upper Delaware Bay, New Jersey. Using spectral analysis, they find that the ratio of the freeboard to incoming wave height is a critical factor such that wave dissipation intensifies as freeboard increases beyond 1.6 times the incoming spectral significant wave height. This study also shows that long swell waves do not experience dissipation by these oyster reefs. Similarly, Safak et al. (2020) show that wave dissipation decreases as water level increases with respect to the two nature-based breakwalls examined in their study, while the more porous breakwall induced smaller wave dissipation. Each of these studies investigated a single type of living shoreline. To the best of our knowledge, there is no published work that compares the wave attenuation between different living shorelines in the same wave climate.

Our study was motivated by the question of how different living shorelines attenuate waves once subjected to the same wave conditions. We identified a study site where a marsh sills and an array of oyster reef balls, referred to as ORB hereafter, were implemented along the same shoreline. A marsh + stone sill, referred to as MSS hereafter, is composed of a low elevation stone structure that can dissipate low to medium wave energy. The shoreline behind the sill is filled with sediment and planted to stabilize the reclaimed land. ORBs function similar to low-crested stone breakwaters and are suitable for low to medium wave energy setting but are designed to attract and grow oysters. Marsh sills are the most widely implemented living shoreline type in Virginia, and there is a growing interest in oyster reefs for the State's rivers and coastal bays due to oyster's substantial capacity for enhancing water quality (Kellogg et al. 2013). In this study, we measured waves at both sides of these features and quantified spectral wave dissipation by each. The results of this study could inform future decisions on implementation of these features as shoreline management strategies.

Methods

Study Area

The living shorelines explored in this study were located on the Lafayette River in Norfolk, Virginia. Around 40% of Norfolk's residents live along this river. The study site was located along the coast of the Heritage Museum and Gardens and within the area where two living shoreline types, MSS and ORBs, were implemented. In 2010, 40 ORBs were placed in the study area along the shoreline as a larger effort to restore oyster habitat in the Lafayette River and protect the shoreline against erosion. Subsequently, in 2018, the Lafayette River became the first river in Virginia to meet oyster habitat restoration goals, and these efforts have revitalized 80 acres of oyster reefs on the river (Chesapeake Bay Foundation 2017). The Lafayette River is tidally influenced by the Elizabeth River. The ORBs have a height of 18 inches and a two-foot diameter and were placed six feet from the shoreline. The crest height of the ORBs was 0.45 mabove the riverbed and only 2 cm above MSL. The MSS project in the study area was funded by the National Oceanic and Atmospheric Administration (NOAA Habitat Blueprint) and entailed

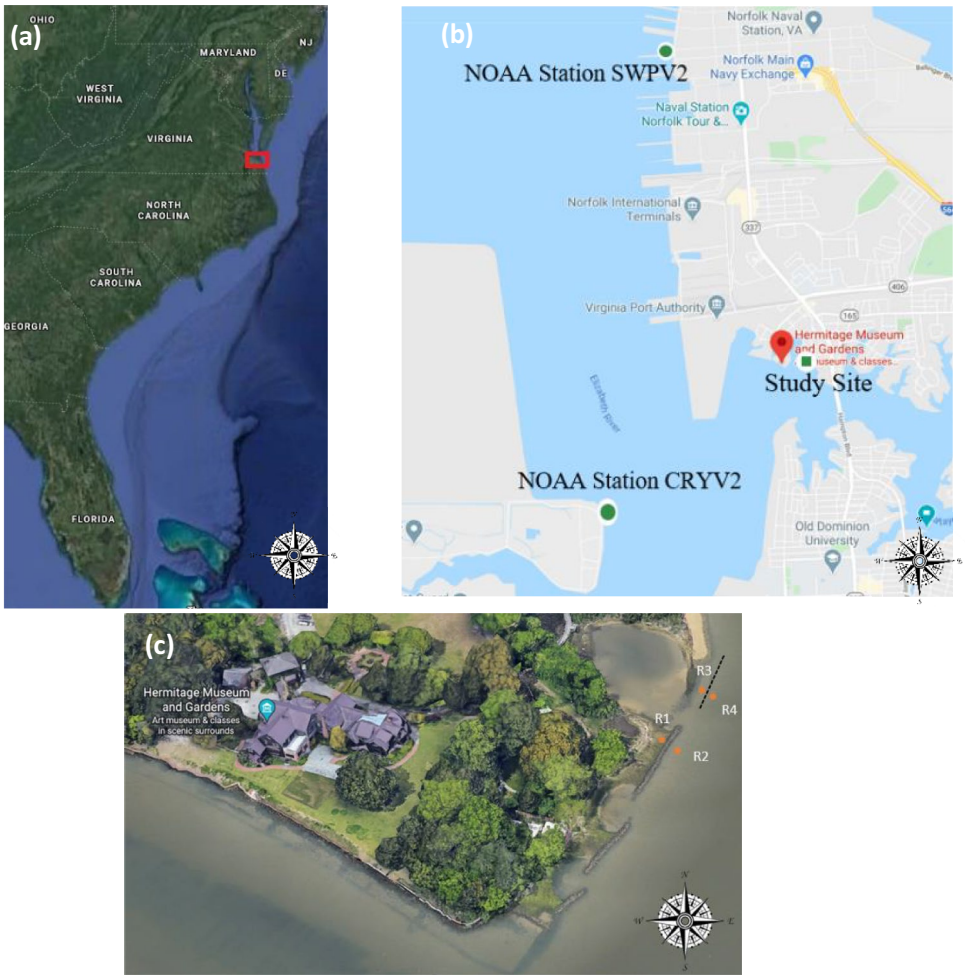

Fig. 1 **a** Map of the East Coast of the USA indicating the study area in Norfolk, VA (red rectangle), **b** location of the living shorelines and the nearby NOAA tide and meteorological stations, and **c** layout of wave sensor deployment from September 23 to October 18, 2019. Sensor R1 and R2 were around the marsh sill and R3 and R4 at around the reef balls which are indicated as a black dotted line (Source: Google Maps)

restoration of 0.5 acre of wetlands and implementation of MSS along 300 ft of shoreline. Figure 1 shows a map indicating the geographical location of the study area and location of the wave gages. The crest height of MSS was measured to be approximately 1 m. The MSS crest was 0.58 m above the MSL. Figure 1c shows the layout of the deployment.

Figure 2 shows the pictures of the MSS and the ORBs in the study site during a low tide. The tide in the study area was semi-diurnal, and its amplitude ranged from 0.12 to 0.91 m during the deployment time. Both structures were submerged during high tide and exposed during low tide although the ORBs were submerged more frequently due to lower crest elevation. The structures were in proximity (~ 20 m apart) and thus were impacted by nearly the same water level and wave conditions. Figure 2 shows these two features at the study site during a low tide. Four RBR

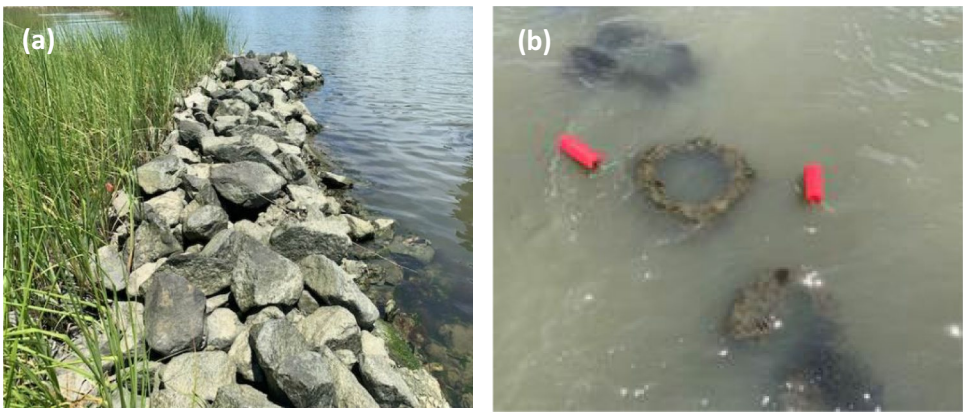

Fig. 2 **a** Marsh sill and **b** oyster reef balls at the study site in Lafayette River, Norfolk, Virginia

SoloD|Wave pressure sensors were deployed at the riverbed around the structures from September 23 to October 18, 2019. The distance from the offshore and onshore gages at both MSS and ORB was nearly 1 m (Fig. 1c). Due to the curvature of the shoreline, the orientation of the stone sill and the ORBs were not the same. While waves approach MSS nearly normal to the shore, they approach ORBs at a nearly 45° angle corresponding to the direction of the dominant fetch. Therefore, the wave sensors around ORBs were placed along a 45-degree line with respect to the shoreline to align with the direction of the incoming waves.

Wind Field

The wind climate was obtained from a nearby NOAA meteorological station (station CRYV2; Fig. 1b) located at about 3.3 km southwest of the study site. The anemometer is 9.6 m above MSL. The dominant wind speed in the study area was approximately 2–4 m/s and primarily from southwest, which is the direction of the dominant fetch in the study area. Secondary winds from northwest also impacted the area and had higher speed, with the maximum reaching approximately 14 m/s, as shown in a wind rose in Fig. 3a. A time series of wind vectors, wind speed, and speed and wind vectors are plotted in Fig. 3b, c.

Wave Analysis

The pressure was measured at 8 Hz continuously over the deployment period. The recorded pressure is the absolute pressure consisting of the gage pressure (p) and the atmospheric pressure (p_{atm}). The absolute pressure was converted to water depth as $h_s = (p - p_{atm})/\rho g + d$ where h_s is water depth corresponding to hydrostatic pressure, ρ is water density, g is gravity, and d is the elevation of the sensor from the bottom. The mean water depth (h) is averaged out, and a pressure

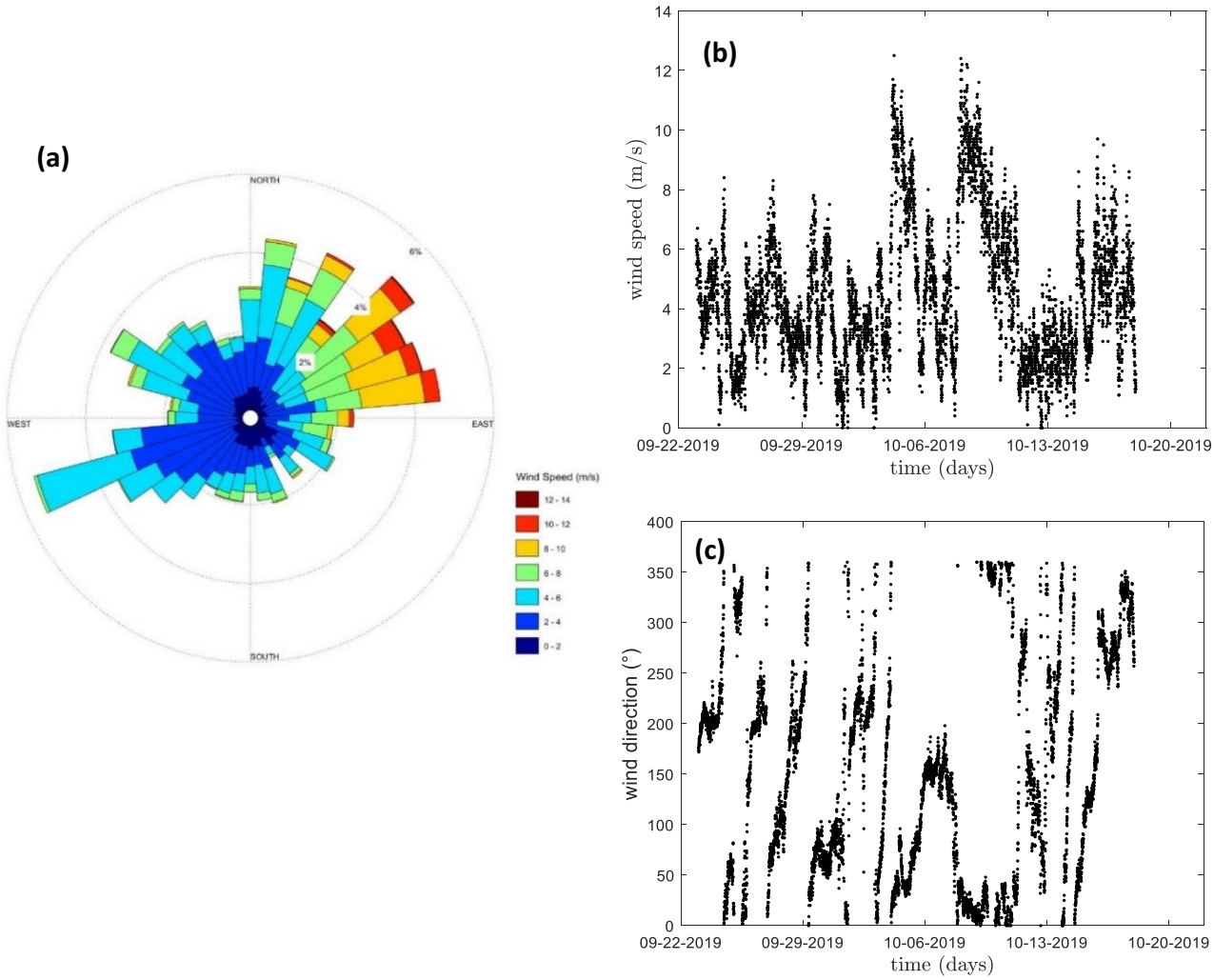

Fig. 3 **a** Wind rose, **b** wind vectors, and **c** wind speed for the 27-day period of deployment

correction factor (K_p) is applied to calculate wave amplitude (a) using pressure at the riverbed (p_d) to account for the profile of dynamics pressure (Dean and Dalrymple 1991):

$$a = \frac{p_d}{\rho g K_p(-h)} \tag{1}$$

where K_p is given by:

$$K_p(-h) = \frac{1}{\cosh(kh)} \tag{2}$$

The Ocean Wave Analysis Toolbox OCEANLYZ (Karimpour and Chen 2017) was used to analyze the pressure data and extract spectral wave properties. The minimum and maximum cut-off frequencies were set to 0.04 Hz and 1 Hz, respectively. The spectral analysis outputted the zero-moment wave height (H_{m0}), mean wave period (T_{m0}), peak wave period (T_p), and wave power density spectrum ($S_{\eta\eta}$). Spectral significant wave height is calculated for each burst using the spectrum as:

$$H_{m0} = 4\sqrt{m_0} = 4\sqrt{\int_0^\infty S_{\eta\eta}(f)df} \tag{3}$$

where m_0 is the zeroth moment of the spectrum and f is the frequency. The peak wave period can be calculated using the peak frequency (f_p), which is associated with the maximum value of $S_{\eta\eta}$,

$$T_p = \frac{1}{f_p} \tag{4}$$

Since the measured H_{m0} were small, we examined the error in H_{m0} and against the sensor error to ensure that reported values are reliable. Although the dataset was continuous, 30-min bursts were defined, and each spectral wave height was calculated over one burst. The atmospheric pressure is averaged over the time when a sensor was exposed, and the offset is subtracted from the total pressure to calculate the gage pressure. Since the propagation of error from water level measurements in time domain to calculated H_{m0} values in frequency domain is not straightforward, we calculated the time-domain significant wave height (H_s = the average of top 1/3 of wave heights in a burst) using the zero up-crossing method and the data from gage R4 as an example. Our analysis based on zero up-crossing method shows that on average, there were 237 waves in a burst. Based on manufacturer specifications, the sensor error is at the order of 1 cm, and since H_s is averaged over 91 waves, the error in H_s is $1/\sqrt{91}$ cm or 1.1 mm. Furthermore, comparison of H_s and H_{m0} values showed that they were nearly identical with RMSE of 0.136 mm; thus, our error calculations for H_s apply to H_{m0} even though the error calculations are not exactly applicable to frequency-domain measurements. Among the wave heights measured by R1 and R2 gages, 4.20% and 3.96% were under 1.1 mm, respectively (excluding zero wave heights which correspond to the time R1 was exposed), while no H_{m0} values from R3 and R4 fell under this threshold. Consequently, despite the observed waves being generally small, averaging over bursts and subtracting the pressure offset ensure that nearly all H_{m0} measurements are above the sensor error and bias is eliminated from the measurements.

The spectral significant wave heights from each gage were calculated, and the difference between the onshore and offshore gage around each structure was used as a measure for wave dissipation. Subsequently, the reduction of wave height by the features was compared. Furthermore, wave energy dissipation for each frequency was computed to examine dissipation across the spectrum. The rate of wave energy dissipation for frequency i (f_i) is given by,

$$\varepsilon_i = \frac{F_{i,shoreside} - F_{i,offshore}}{\Delta x} \tag{5}$$

where $F = \frac{1}{2}\rho g a_i^2 c_{g,i}$ is the energy flux, ρ is water density, g is gravity, $C_{g,i} = \frac{\omega_m(i+1)-\omega_m(i)}{k(i+1)-k(i)}$ is wave group velocity, ω is angular frequency, and $a_i = \sqrt{2S_{\eta\eta}(f_i)df}$ is the spectral wave amplitude.

A threshold based on rate of wave transmission was used to categorize the results. Based on laboratory experiments on low-crested breakwaters, Van Der Meer et al. (2005) showed that relative magnitude of incoming wave height to the freeboard over structure crest is a critical factor for wave transmission. Based on this study and similar to the criterion used by Zhu et al. (2020), we set the threshold to $R = (H_{m0})_{offshore}/\delta = 0.625$, where δ is the freeboard (Fig. 4). High wave transmission (low dissipation) occurs when $R < 0.625$, while low wave transmission (high dissipation)

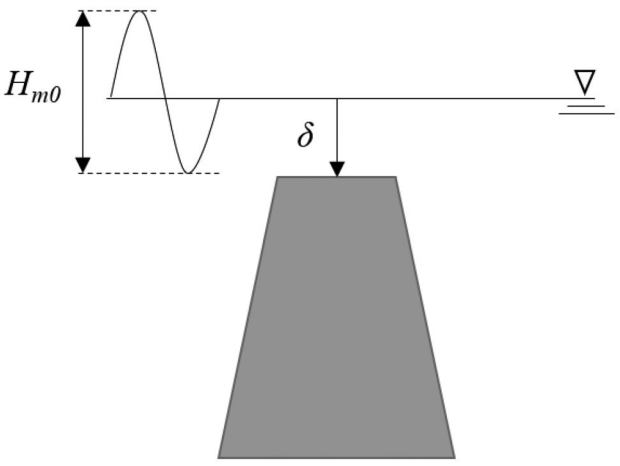

Fig. 4 Relative wave height with respect to freeboard is used to categorize results based on wave transmission

occurs when $R > 0.625$. The structure crest is exposed when $R < 0$, and it is submerged when $R > 0$. The threshold was calculated using the significant wave heights measured at the sensor on the offshore side of each structure.

Results

Water Depth and Bulk Wave Characteristics

The variation in water depth around each structure is shown in Fig. 5. The average water depth at the offshore and shore sides of MSS were 0.79 m and 0.39 m, respectively, and it was 1.07 m on both sides of the ORBs. Variation of spectral significant wave height and peak period offshore of the marsh sill is shown in Fig. 6. The average tide range was measured at 0.77 m, and the average significant wave height offshore (gage R2) and shore side (gage R1) of MSS around the sill were 0.0190 m and 0.0116 m, respectively. The maximum significant wave height at these two locations was 0.0872 m and 0.0671 m, respectively. The average significant wave heights offshore (gage R4) and shore side (gage R3) of the ORBs were 0.0184 m and 0.0210 m, correspondingly, and the maximum significant wave heights at these gages were 0.10 m and 0.08 m, respectively. As expected, waves are smaller on the shore side of each structure due to dissipation, and that MSS dissipates waves more strongly compared to ORBs. The average T_p offshore and onshore of the marsh sill is 2.86 s, and 3.96 s, respectively, while it equals 2.52 s and 2.63 s offshore and onshore of the ORBs, respectively.

Wave height is affected by both water level and wind speed. High water levels allow for larger waves to propagate without breaking and create a larger freeboard over structure crests allowing transmission of larger waves. This effect is evident in Fig. 6 where waves in the shoreside of the MSS and ORBs are comparable to those on the offshore side during October 7–10, 2019. This time corresponds to highest water level observed during the deployment (Fig. 5). On the other hand, high waves observed from October 18–20, 2019, correspond to sustained moderate wind activity over this period (Fig. 3). Small peak periods and wave height indicate that waves are the result of small fetch in the area and show that waves are locally generated wind waves.

The cumulative probability distribution function (CDF) of wave heights measured offshore of MSS and ORBs is similar. The average T_p offshore of the two features is also close. These findings confirm that both features are impacted by statistically equivalent waves (Fig. 7), as was expected due to their proximity. Furthermore, the CDF at the shoreside of the two features clearly shows wave dissipation and indicates that MSS dissipates waves more strongly than ORBs.

Wave Dissipation

The measured wave spectra on the offshore and onshore sides of both features clearly indicate wave attenuation. Figure 8 shows the averaged wave spectra over the entire duration of deployment. The peak energy is at $f_p = 0.57$ Hz at the offshore gages as seen in the figure, which persists to be the peak in the damped frequency onshore of MSS and ORBs. A secondary peak at 0.38 Hz is observed at the incoming and damped spectra around both features. Comparing the

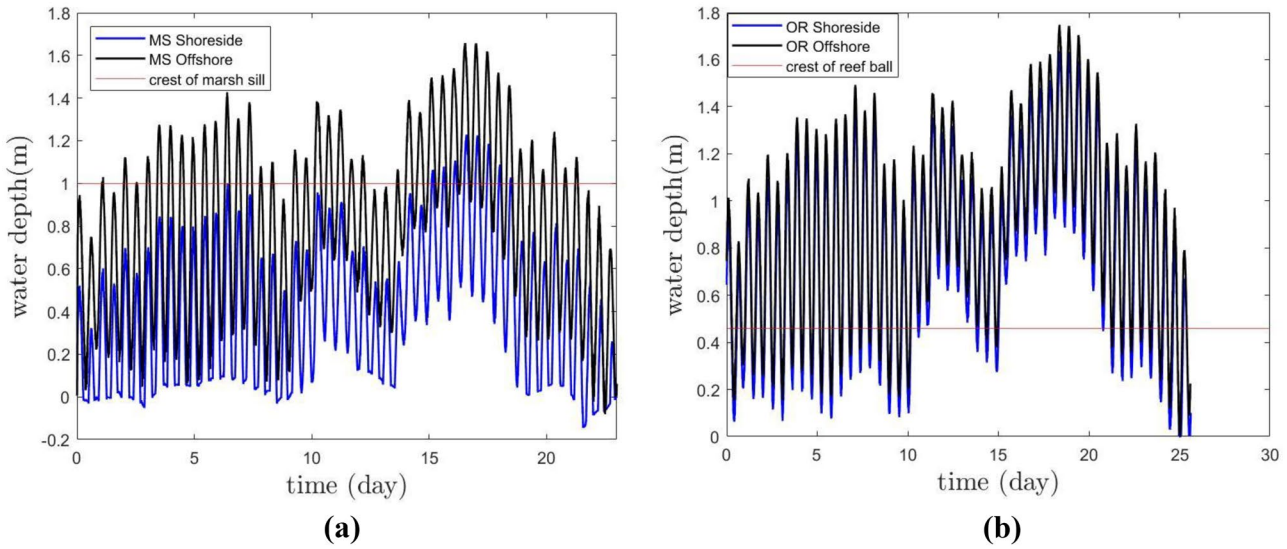

Fig. 5 Variation of water depth at the shore and offshore side of **a** Marsh + stone sill (MSS) and **b** oyster reef ball (ORB). Red lines indicate the crest of each structure

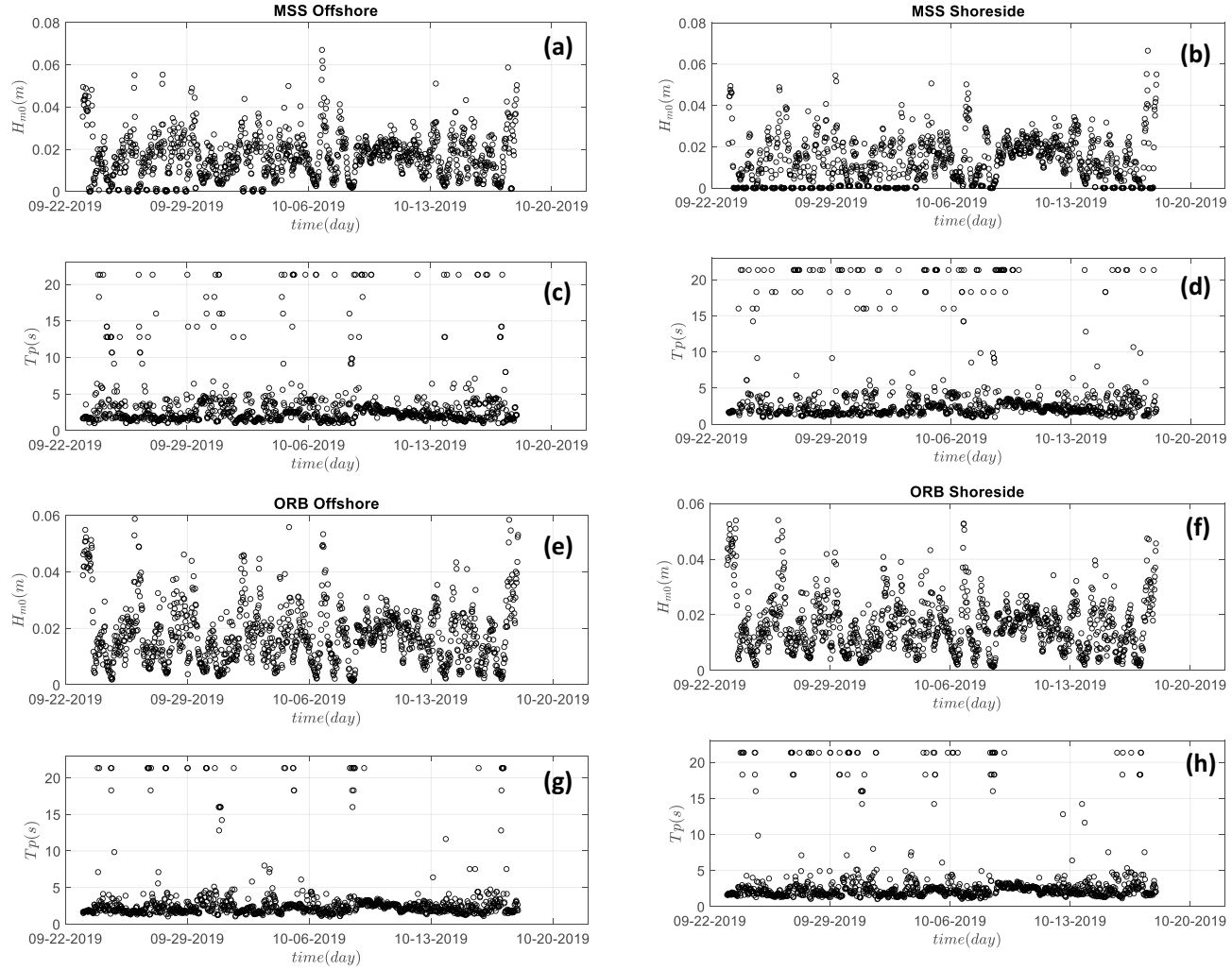

Fig. 6 Significant wave height and peak wave period measured offshore and shoreside of MSS (**a**–**d**) and ORBs (**e**–**h**)

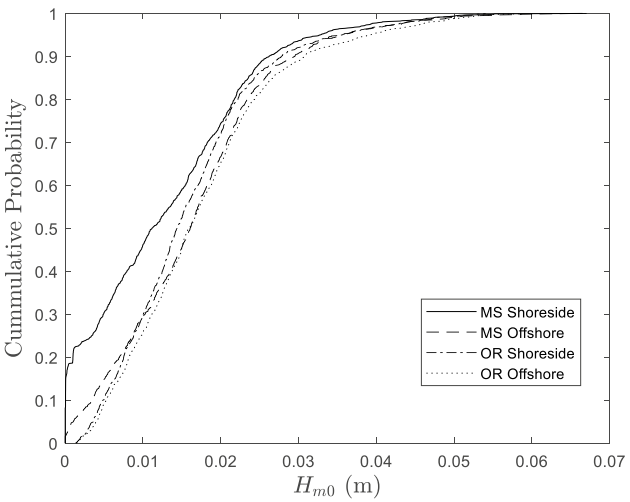

Fig. 7 Cumulative probability distribution of measured significant wave height around MSS and oyster reef balls (ORBs)

damped spectra shows that MSS dampens the peak and its surrounding frequencies at a stronger rate compared to ORB. For example, the peak frequency is damped by MSS and ORB by 35% and 26%, respectively.

As discussed in the "Methods" section, wave dissipation depends on the ratio of the height of the incoming wave to the free board (δ; Fig. 4), and the threshold $R = 0.625$ is applied to delineate wave dissipation as a function of free board over the structure crest. δ ranged from − 0.648 to 1.05 m for MSS and − 1.474 to 0.429 m for ORBs. The sill and the reef balls were fully submerged during 28% and 94% of the deployment, respectively.

Wave dissipation strongly depends on the freeboard. Figure 9 shows the variation of H_{m0} around each feature for different R values. Note that δ differs between MSS and ORBs due to difference in water depth around the two features (Fig. 5). The MSS feature and ORBs show an average dissipation of 38% and 11%, respectively, over the entire

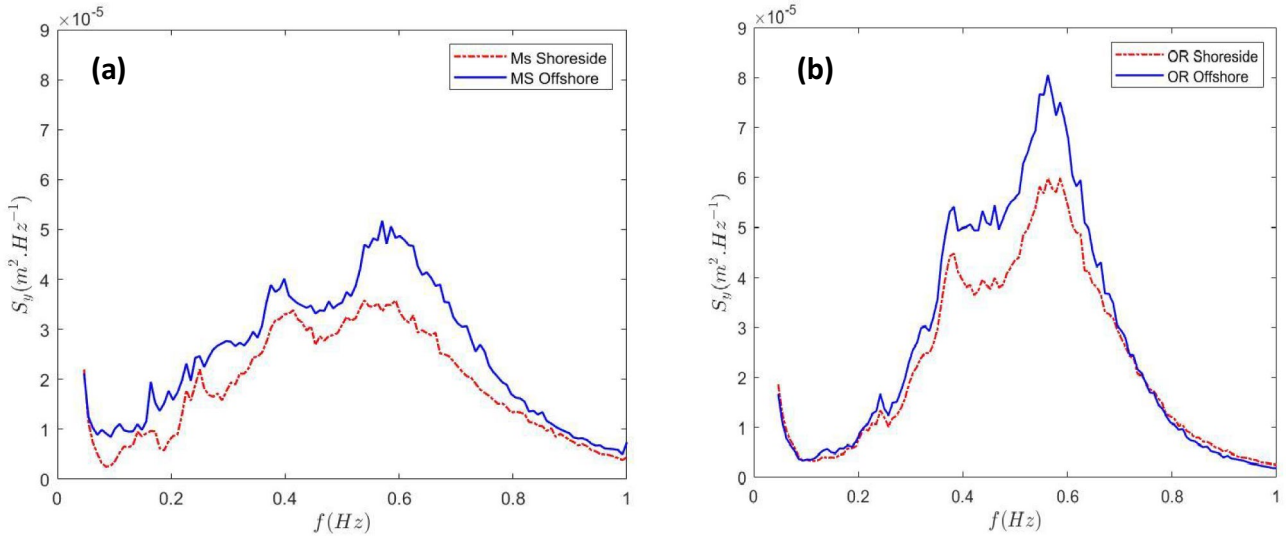

Fig. 8 Wave spectra on the offshore and onshore sides of **a** marsh sill and **b** oyster reef balls for the full duration of the deployment

dataset. To further investigate the effect of the freeboard, a least-square line is fitted to the scatter plots, and its slope indicates how much wave height is reduced over each feature for different ranges of R. The features become emergent or near emergent at low tide, corresponding to small δ and $R > 0.625$, resulting in relatively high dissipation rates.

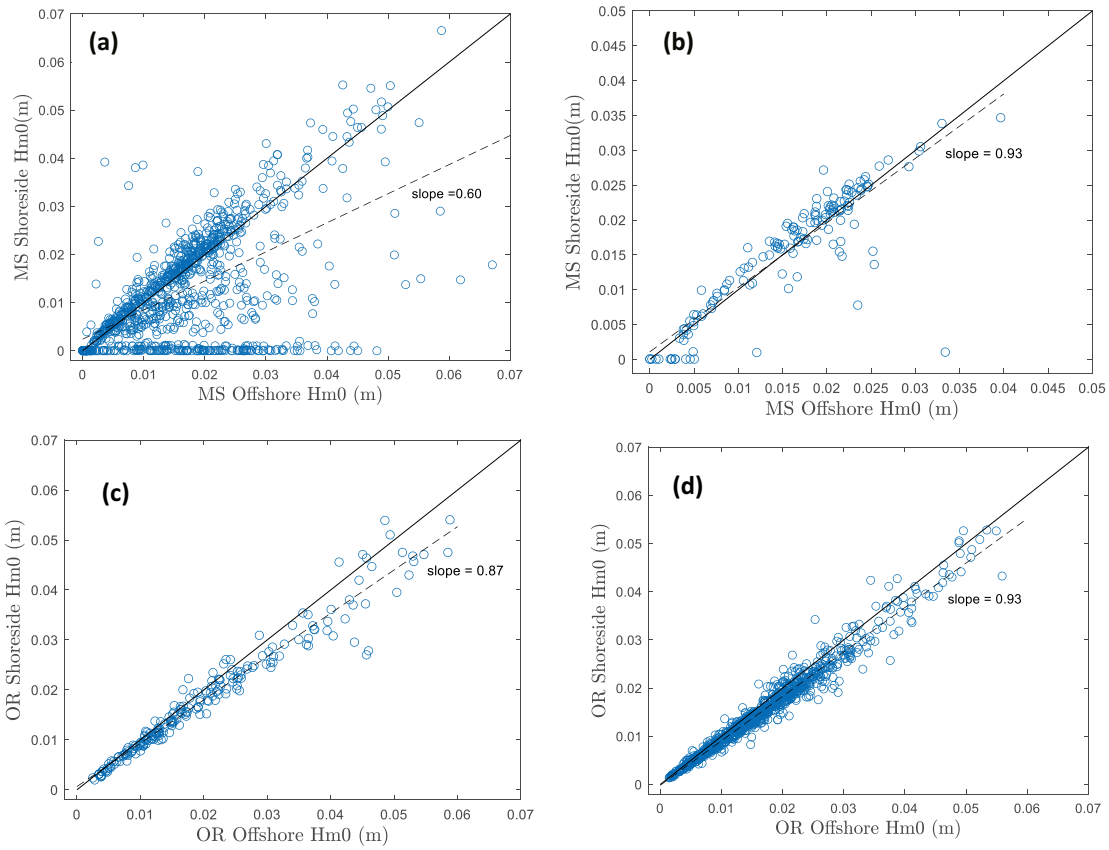

Fig. 9 Significant wave height for the offshore and shore side sensors for $R > 0.625$ (**a** and **c**) and $R < 0.625$ (**b** and **d**) for MSS (**a** and **b**) and for ORBs (**c** and **d**). The linear least-square lines and their slopes are shown

Under this condition, MSS and ORBs reduce wave height by 40% and 13%, respectively (Fig. 9a, c). The wave reduction in shoreside of the features is attributed to wave dissipation by the structure, depth-limited breaking, and partial wave reflection. Higher wave dissipation over MSS compared to ORBs when $R > 0.625$ is attributed to three factors. First, the ORBs are more permeable than stone rock sills. Second, the depth on the shoreside of the sill is smaller compared to shoreside of the reef balls due to a sand fill and thus can support smaller waves due to depth-limited breaking. Third, the gaps between the reef balls allow waves to transmit through the ORBs, while MSS is a continuous feature where wave reflection from armors in the sill likely results in breaking of waves over other armors rather than wave transmission; thus, MSS blocks the waves more efficiently.

In some wave bursts, 100% dissipation was observed over MSS which corresponded to exposure of the shoreside gage during some of the low tides. Such observation was not made for ORBs as both sides of the bed on both their sides were submerged all the time. As water level increases, the difference between the efficiency of the two features in wave dissipation vanishes such that for $R < 0.625$, the average wave dissipation rate for both features is 7% (Fig. 9b, d). As seen in Fig. 9, more data points exist in this range for ORBs than MSS as MSS has a higher crest.

Figure 10 shows the frequency-dependent dissipation as averaged over wave bursts that make up the entire duration of deployment. The results show that the highest dissipation occurs at the spectral peak, $f_p = 0.57$ Hz. Furthermore, it is observed that while the spectrum undergoes highest damping at the range of $f = 0.3$–0.6 Hz over ORB, MSS damps waves more evenly across the spectrum such that lower frequencies experience substantially higher damping compared to ORBs. High frequencies also experience higher attenuation over MSS compared to ORB.

Figure 11 shows the probability distribution and cumulative distribution of percent dissipation of significant wave height, defined as $[(H_{m0})_{offshore}\text{-}(H_{m0})_{shoreside}]/(H_{m0})_{offshore}$, for the two features. As seen, the most common rate of dissipation observed for both structures is in the range of 10–20%. The MSS feature also shows a relatively high rate of dissipation at 90–100% range. It is noted that the rate of wave dissipation shows a wider distribution over MSS, in contrast to ORB which does not cause wave dissipation rates larger than 50%. Figure 12 shows the percentage of reduction in transmitted H_{m0} with respect to the incoming H_{m0} for different values of R. As discussed earlier, $R > 0$ and $R < 0$ correspond to conditions where the features are emergent and submerged, respectively. As seen in the figure, wave dissipation percentage over MSS and ORBs is similar once both features are submerged, consistent with Fig. 9b, d. Conversely, MSS results in much stronger wave dissipation than ORB if both features are emergent.

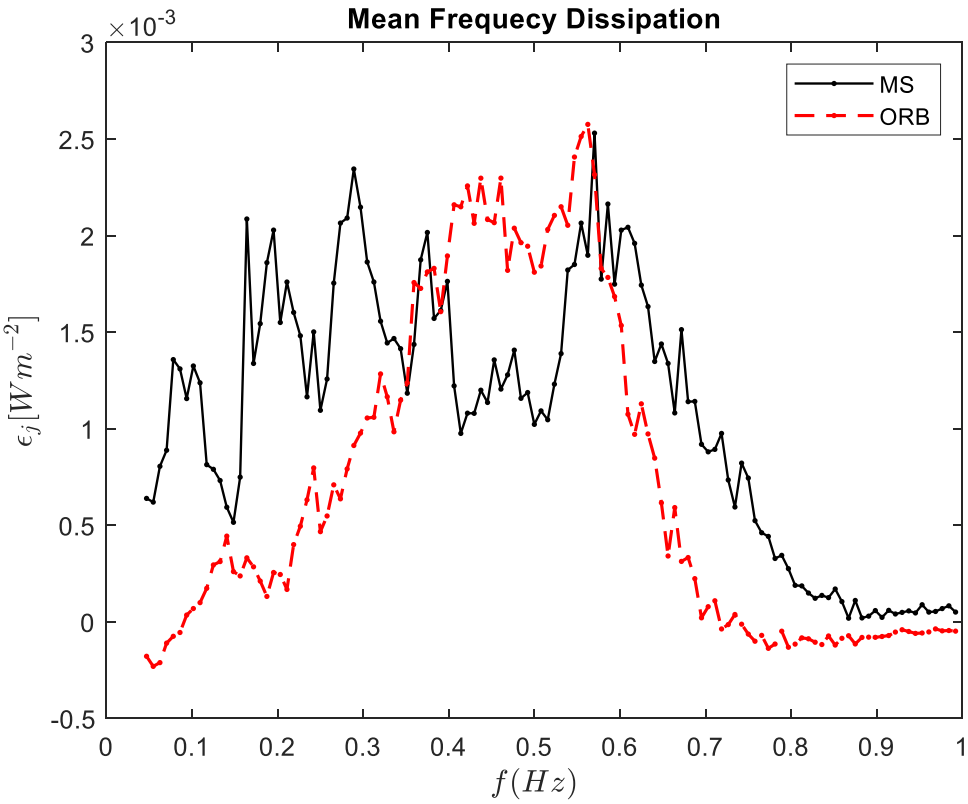

Fig. 10 Frequency-dependent dissipation across the spectrum averaged over wave bursts

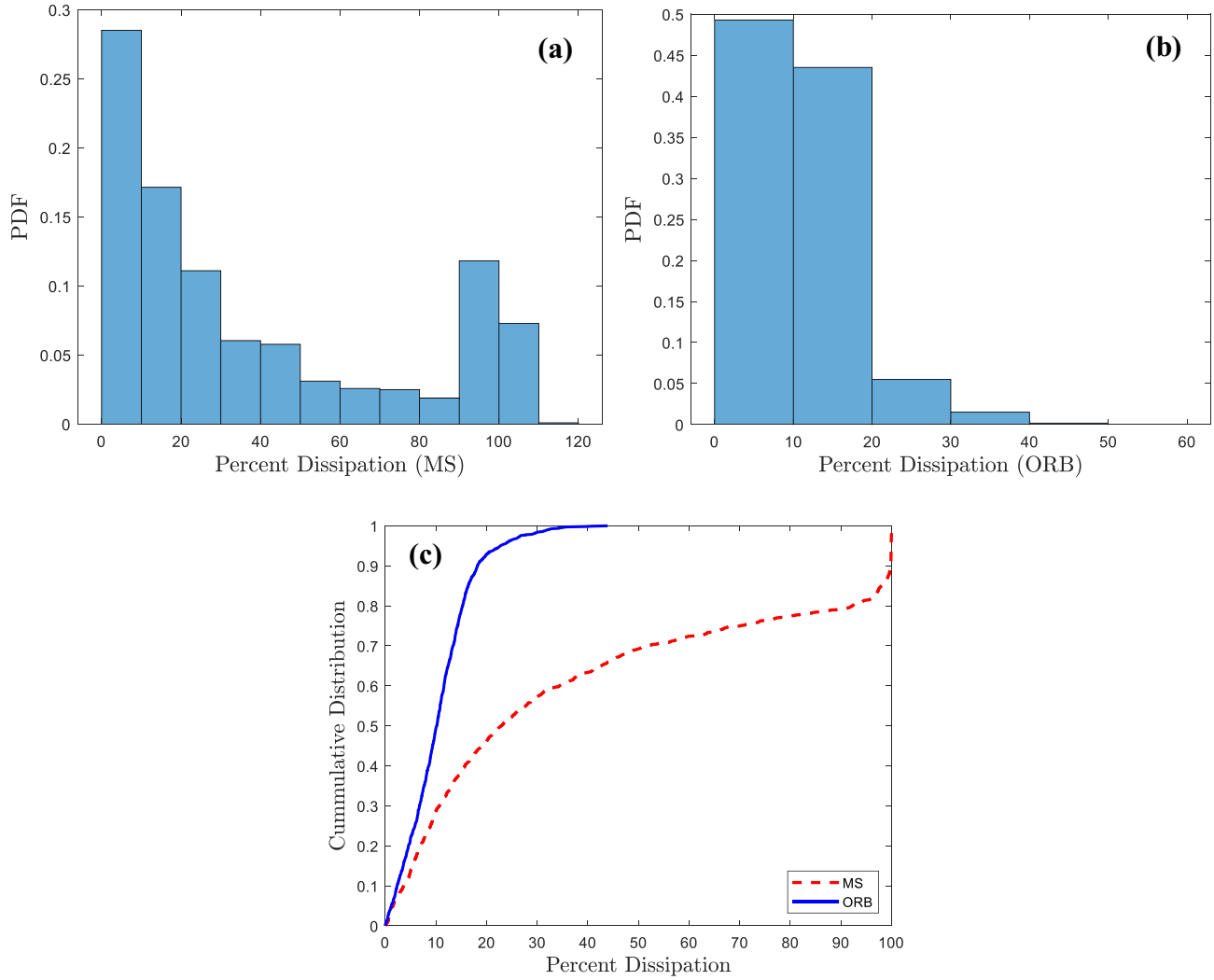

Fig. 11 Probability distribution of dissipation percentage of significant wave height over **a** MSS and **b** ORBs and **c** cumulative probability distribution of percentage reduction in significant wave height

Discussion

Harmonic Generation

The waves that affect the study site are locally generated by winds with a peak at 0.57 Hz, and the MSS feature was found to be generally more efficient in dissipating waves across the wave spectrum. An interesting observation over MSS was the secondary high dissipation rates at subharmonic frequencies of the peak frequency such that the second highest dissipation is observed at $f = 0.28$ Hz $= f_p/2$ followed by the third highest dissipation at $f = 0.16$ Hz $\approx f_p/4$. The frequency $f = 0.078$ Hz ($f_p/8$) also exhibits relatively high dissipation among low frequencies.

This pattern suggests energy transfer from low to high frequencies through superharmonic interactions over the MSS.

Effects of Wave Shoaling, Breaking, and Reflection

It should be noted that in addition to structural differences between the two features, the bathymetry and topography around them differ, and this can affect wave transformation. The ORBs are constructed on the riverbed, and the bathymetric elevation offshore and onshore of these features are the same. In contrast, the onshore side of the sill where the marsh is planted is filled with sand and elevated. The higher elevation of the marsh results in wave shoaling which can enhance wave breaking and dissipating compared to ORBs. Thus, higher efficiency of MSS in wave dissipation compared to ORBs could partially be due to shoaling and subsequent wave breaking in the marsh. To quantify the effect of shoaling and wave breaking, we use the linear wave theory to calculate the predicted significant wave height in the absence of MSS

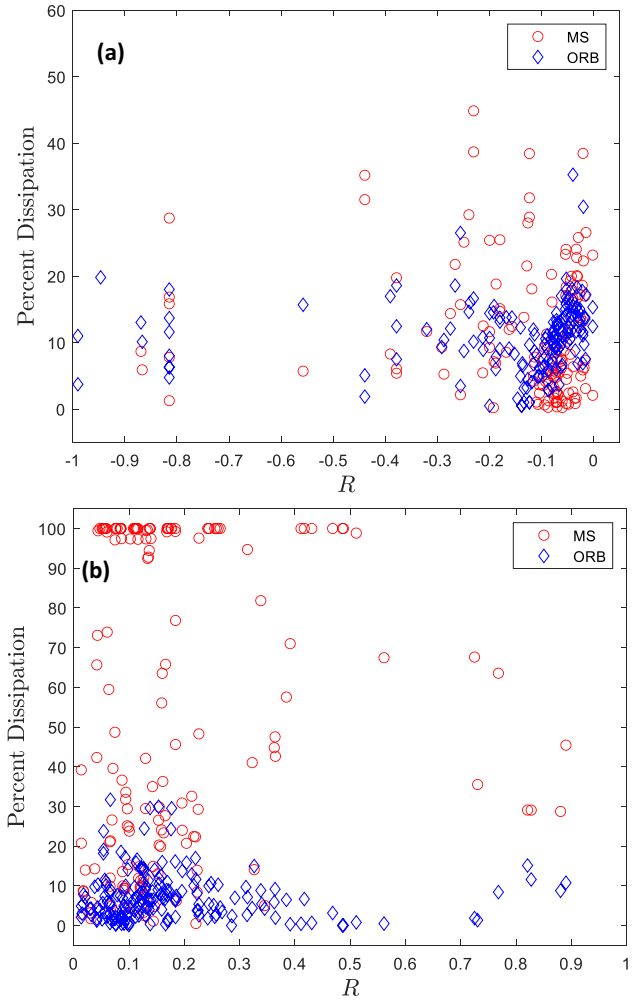

Fig. 12 Variation of wave dissipation percentage (relative to the incoming wave height) against relative crest height (R). Structures are **a** submerged and **b** emergent

based on incoming wave information and compare the results with the measured significant wave height onshore of MSS. The shoaling coefficient is calculated as (Dean and Dalrymple 1991):

$$K_s = \sqrt{\frac{C_{g,off}}{C_{g,shore}}} \tag{6}$$

where $C_{g,off}$ and $C_{g,shore}$ are wave group velocities offshore and shoreside of MSS, respectively. Wave celerity is estimated using the formulation of Hunt (1979), which is then used to calculate C_g. In the absence of sufficient information on local bathymetry, refraction effects are ignored, and the predicted wave height shoreside of MSS ($H_{m0,\,pred}$) is calculated as:

$$H_{mo,\,pred} = K_s H_{mo,\,off} \tag{7}$$

where $H_{m0,\,off}$ is the spectral significant wave height offshore the MSS. The effect of wave breaking is also considered by imposing depth-induced breaking limit of 0.78. This limit is used to eliminate significant wave heights larger than 0.78 of the time-averaged depth from the record. The measurements that were below the accuracy threshold for the significant wave height are omitted including zeros recorded during low tides where shoreside of MSS was exposed. Figure 13 shows the variation of $H_{m0,\,shoreside}$ against $H_{m0,\,pred}$ around the MSS. The slope of the line (0.73) indicates that 27% of the wave height attenuation can be attributed to the stone sill. This result agrees with observations of Morris et al. (2021) for wave attenuation over rock sills in their Virginia sites.

Wave reflection can affect measurements, and location of gages can be selected to minimize this effect. However, other considerations can also influence gage placement. The motivation to place gages in the immediate vicinity of the structures were to isolate the effect of structures on wave dissipation and eliminate the effects of wave refraction, bottom roughness, and vegetation on wave heights. R1 could not be placed further away as wave dissipation calculations would have been complicated by the impact of vegetation marsh. R3 was a few meters away from the marsh edge on its shoreside; thus, we do not anticipate wave reflection to affect its measurements. As seen in Fig. 9c and d, wave heights on offshore and shoreside of ORBs are comparable. Noting that water depth does not change around ORBs and thus there is no shoaling effect, we conclude that the effect of reflection from ORBs should be minimal. Porous breakwaters damp short waves more efficiently than the long waves, and since the observed waves are dominantly short (Fig. 8), we expect that they are much more strongly damped than reflected by the stone sill. In general, to minimize wave reflection, wave gages can be placed several wave lengths away from reflective surfaces. In doing so, however, potential effects of other frictional elements including bottom sediments or aquatic vegetation should be considered.

Permeability of Structural Features

It would be instructive to evaluate the permeability of structural features of different types. Van der Meer and d'Angremond (1991) provide an equation for wave transmission coefficient through porous breakwaters as a function of incoming wave height, offshore wave steepness, freeboard, crest width, and mean rock size. Based on their study, as the mean rock size increases, wave transmission coefficient increases or wave attenuation decreases. Although ORBs in this study were more permeable than the stone sill, both features showed comparable wave transmission when submerged. When emergent or near-emergent, however, the stone sill exhibited lower transmission as expected. The porous

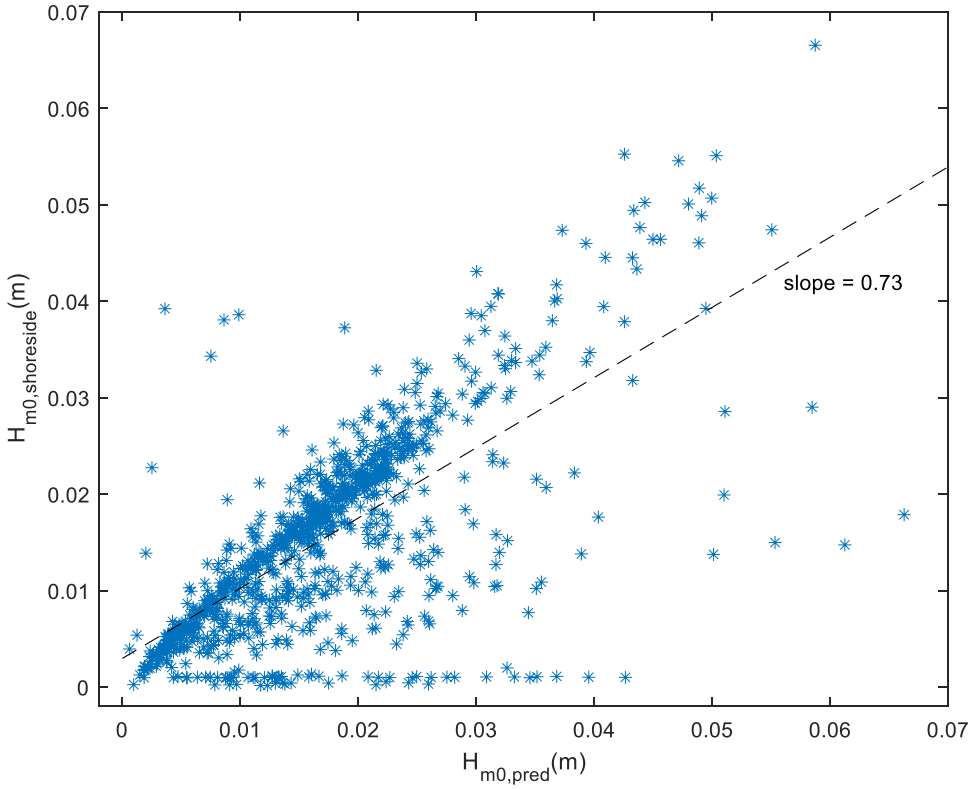

Fig. 13 Measured significant wave height shoreside of MSS compared to the predicted values that consider shoaling and breaking effect

breakwaters investigated in Van der Meer and d'Angremond (1991) do not represent the highly permeable oyster reef balls in this study, and to our knowledge, there is no study that compares wave transmission through permeable structures of different types. This could be the subject of a future study.

Summary and Conclusion

Waves were measured around two widely used living shorelines features, namely a marsh sill and an array of oyster reef balls, in a sheltered bay. The two features were built to stabilize the shorelines of the Hermitage Museum and Gardens property along the Lafayette River, and a comparison of their performance in attenuating wave energy was possible since they were in the same wave environment. The sheltered small estuarine/riverine environment that this property is located on represents typical properties that are good candidates for nature-based shoreline stabilization features; thus, findings from this study can be widely applicable. Four pressure sensors were deployed on the offshore and onshore sides of each structure for 27 days in September and October of 2019. The waves in the study area were generally small with a maximum of 9-cm wave height measured during the deployment. The MSS and the ORBs were submerged 28% and 94% of the deployment time, respectively.

Similar to observations in earlier studies (Van Der Meer et al. 2005; Zhu et al. 2020), our measurements indicate that wave attenuation depends highly on the ratio of incoming significant wave height to the free board. Although MSS was more dissipative in general due to higher crest elevation and an elevated marsh behind, the two features caused comparable wave dissipation once they were submerged, and the free board was larger than 0.625 of the incoming significant wave heights. It is noted that ORBs are constructed with low crests to provide favorable condition for oyster settlement and growth which occurs in subtidal or intertidal conditions, and thus constructing them with high crest will diminish their ecosystem functions. Higher wave attenuation can be achieved by constructing multiple lines of ORBs, and the small footprint of ORBs compared to MSS can support this approach. Future studies can examine the number of rows, arrangement, and dimension of ORBs that can provide dissipation rates that are comparable to high-crested MSS features.

Future work can involve numerical simulation of wave dissipation over MSS and ORBs, their combination, or other alternative to achieve optimal design for wave dissipation and habitat services. Furthermore, in the absence of control site, numerical models can differentiate between damping due to structures and the morphology of the shorelines. Finally, the purpose of living shorelines is to reduce erosion and stabilize the coastline. Future work can assess how these features affect sediment resuspension by waves and how the

resuspension results in shoreline erosion or accretion around these features.

Acknowledgements We appreciate Jackie Shannon from the Chesapeake Bay Foundation for her assistance in identifying the study site and the Hermitage Museum and Gardens for providing access to living shorelines in their property. AL appreciates the support from the Department of Ocean, Earth and Atmospheric Sciences at Old Dominion University during her REU study. Some of the instruments and supplies used in the study were obtained through funding from a Virginia Sea Grant Graduate Fellowship.

Funding This work was funded by the National Science Foundation's Research Experience for Undergraduates (REU) Program.

Declarations

Competing Interests The authors declare no competing interests.

References

Chesapeake Bay Foundation. 2017. Chesapeake Bay Foundation-Lafayette River restoration. Retrieved February 28, 2021, from https://www.cbf.org/how-we-save-the-bay/programs-initiatives/virginia/hampton-roads/lafayette-river-restoration/.

Coen, L., R. Brumbaugh, D. Bushek, R. Grizzle, M. Luckenbach, M. Posey, S. Powers, and S. Tolley. 2007. Ecosystem services related to oyster restoration. *Marine Ecology Progress Series* 341: 303–307.

Davis, J.L., C.A. Currin, C. O'Brien, C. Raffenburg, and A. Davis. 2015. Living shorelines: Coastal resilience with a blue carbon benefit. *PLoS ONE* 10 (11): e0142595.

Dean, R.G., and R.A. Dalrymple. 1991. Water wave mechanics for engineers and scientists, world scientific publishing company.

Dean, R.G., and R.A. Dalrymple. 2004. *Coastal processes with engineering applications*. Cambridge University Press.

Emanuel, K.A. 2013. Downscaling CMIP5 climate models shows increased tropical cyclone activity over the 21st century. *Proceedings of the National Academy of Sciences* 110 (30): 12219–12224.

Hunt, J.N. 1979. Direct solution of wave dispersion equation. *Journal of Waterway, Port, Coastal, and Ocean Engineering* 4: 457–459.

Karimpour, A., and Q. Chen. 2017. Wind wave analysis in depth limited water using OCEANLYZ, A MATLAB toolbox. *Computers & Geosciences* 106: 181–189.

Kellogg, M., J. Cornwell, M. Owens, and K. Paynter. 2013. Denitrification and nutrient assimilation on a restored oyster reef. *Marine Ecology Progress Series* 480: 1–19.

Leonardi, N., N.K. Ganju, and S. Fagherazzi. 2016. A linear relationship between wave power and erosion determines salt-marsh resilience to violent storms and hurricanes. *Proceedings of the National Academy of Sciences* 113 (1): 64–68.

Living Shorelines Project Map. NOAA Habitat Blueprint. Retreived February 28, 2021, from www.habitatblueprint.noaa.gov/living-shorelines/project-map/.

Marani, M., A. D'Alpaos, S. Lanzoni, and M. Santalucia. 2011. Understanding and predicting wave erosion of marsh edges. *Geophysical Research Letters* 38 (21).

Meyer, D.L., E.C. Townsend, and G.W. Thayer. 1997. Stabilization and erosion control value of oyster cultch for intertidal marsh. *Restoration Ecology* 5 (1): 93–99.

Möller, I., M. Kudella, F. Rupprecht, T. Spencer, M. Paul, B.K. Van Wesenbeeck, G. Wolters, K. Jensen, T.J. Bouma, and M. Miranda-Lange. 2014. Wave attenuation over coastal salt marshes under storm surge conditions. *Nature Geoscience* 7 (10): 727–731.

Morris, R.L., M.K. La Peyre, B.M. Webb, D.A. Marshall, D.M. Bilkovic, J. Cebrian, and S.E. Swearer. 2021. Large-scale variation in wave attenuation of oyster reef living shorelines and the influence of inundation duration. *Ecological Applications* 31 (6): e02382.

Safak, I., C. Angelini, P.L. Norby, N. Dix, A. Roddenberry, D. Herbert, E. Astrom, and A. Sheremet. 2020. Wave transmission through living shoreline breakwalls. *Continental Shelf Research* 211: 104268.

Scyphers, S.B., S.P. Powers, K.L. Heck, and D. Byron. 2011. Oyster reefs as natural breakwaters mitigate shoreline loss and facilitate fisheries. *PLoS ONE* 6 (8): e22396.

Van der Meer, J. W., and d'Angremond, K. 1991. Wave transmission at low-crested structures. In *Coastal Structures and Breakwaters Conference*, 25–42. London: ICE.

Van Der Meer, J.W., R. Briganti, B. Zanuttigh, and B. Wang. 2005. Wave transmission and reflection at low-crested structures: Design formulae, oblique wave attack and spectral change. *Coastal Engineering* 52 (10–11): 915–929.

Whitman, E., and M. Reidenbach. 2012. Benthic flow environments affect recruitment of Crassostrea virginica larvae to an intertidal oyster reef. *Marine Ecology Progress Series* 463: 177–191.

Wiberg, P.L., S.R. Taube, A.E. Ferguson, M.R. Kremer, M.A. Reidenbach. 2019. Wave attenuation by oyster reefs in shallow coastal bays. *Estuaries and Coasts* 42 (2): 331–347.

Zhu, L., Q. Chen, H. Wang, W. Capurso, L. Niemoczynski, K. Hu, and G. Snedden. 2020. Field observations of wind waves in upper Delaware Bay with living shorelines. *Estuaries and Coasts* 43: 739–755.